Critical endpoint behavior in an asymmetric Ising model: Application of Wang-Landau sampling to calculate the density of states

Shan-Ho Tsai,[1,2] Fugao Wang,[1,*] and D. P. Landau[1]
[1]*Center for Simulational Physics, University of Georgia, Athens, Georgia 30602, USA*
[2]*Enterprise Information Technology Services, University of Georgia, Athens, Georgia 30602, USA*
(Received 29 January 2007; published 8 June 2007)

Using the Wang-Landau sampling method with a two-dimensional random walk we determine the density of states for an asymmetric Ising model with two- and three-body interactions on a triangular lattice, in the presence of an external field. With an accurate density of states we were able to map out the phase diagram accurately and perform quantitative finite-size analyses at, and away from, the critical endpoint. We observe a clear divergence of the curvature of the spectator phase boundary and of the magnetization coexistence diameter derivative at the critical endpoint, and the exponents for both divergences agree well with previous theoretical predictions.

DOI: 10.1103/PhysRevE.75.061108 PACS number(s): 05.50.+q, 02.70.Uu, 64.60.Cn, 75.10.Hk

I. INTRODUCTION

Phase diagrams of a diverse range of physical systems, such as binary fluid mixtures, superfluids, binary alloys, liquid crystals, certain ferromagnets, and antiferromagnets, etc., include a critical endpoint (CE), defined as a point in the phase diagram where a critical line meets and is truncated by a first-order transition line. It is widely believed that bulk critical exponents do not change at the CE [1]. This seems most likely to be true but it has hardly been checked beyond phenomenological theory and renormalization calculations [2]. Although critical endpoints are ubiquitous and have been known for a long time [3], new critical behavior has been discovered relatively recently. In 1990, Fisher and Upton [1] defined new universal amplitude ratios for the shape of the first-order phase transition boundary and for noncritical surface tensions near critical endpoints. They have also predicted a new singularity in the first-order phase transition line at the CE. This prediction was confirmed by the Fisher and Barbosa phenomenological studies on an exactly solvable spherical model, which exhibits a critical endpoint for a suitable potential [4].

Later, an extensive Monte Carlo simulation [5] using a multicanonical ensemble method [6] and histogram reweighting techniques [7] was carried out by Wilding to study the critical endpoint behavior in a symmetrical binary fluid mixture [8]. He predicted and observed a singularity on the derivative of the diameter of the liquid-gas coexistence curve as the critical endpoint is approached. Wilding also showed the first numerical evidence of the divergence in the curvature of the spectator phase boundary [8], in accordance with previous theoretical prediction [1,4]. Nevertheless, a quantitative analysis of such singularities at the CE was not done because such analysis would have required much larger system sizes than the ones used, and thereby much more computing power.

In this paper, we study an asymmetric Ising model on a triangular lattice with two- and three-body interactions in an external field [9,10]. The Hamiltonian of the model can be written as

$$\mathcal{H} = -J\sum_{\langle ij\rangle} S_i S_j - J_3 \sum_{\langle ijk\rangle} S_i S_j S_k - H\sum_i S_i, \qquad (1)$$

where $S_i = \pm 1$ is an Ising spin on site i of a triangular lattice, $\langle ij\rangle$ denotes pairs of nearest-neighbor spins, and $\langle ijk\rangle$ represents the three spins on the elementary triangles. The parameters J and J_3 are two- and three-body nearest-neighbor spin couplings, respectively, and H is an external magnetic field. The model is asymmetric because the Hamiltonian is not invariant when $H \to -H$. Periodic boundary conditions are used in this work. Chin and Landau [9] showed that this model is identical to a lattice-gas model; moreover, their Metropolis Monte Carlo simulations revealed that this model exhibits critical endpoints with suitable choices of the coupling parameters. In particular, for $J=1$ and $J_3=2$ the T and H phase diagram has a critical endpoint, which is well separated from the critical point at the end of the first-order transition line.

We perform Wang-Landau sampling [11,12] to determine the phase diagram of this model and to study its behavior at the phase transition lines and at the critical endpoint. Our numerical data not only show the singularity in the phase boundary curvature, predicted by Fisher *et al.* [1,4], and in the magnetization coexistence diameter derivative, predicted by Wilding [8], but also allow us to analyze quantitatively the behavior in the vicinity of the critical endpoint for this model.

II. RANDOM WALK ALGORITHM TO CALCULATE THE DENSITY OF STATES

Conventional Monte Carlo methods [5] generate a canonical distribution at a given temperature T. In contrast, the Wang-Landau method estimates the density of states directly and accurately via a random walk that produces a flat histogram in the random walk parameter space [11–15]. The density of states converges to true values systematically through careful control of a modification factor during the random

*Present address: Intel Corporation, PC1-105, 44235 Nobel Drive, Fremont, California 94538.

walk. A mathematical proof of the convergence of the Wang-Landau method was given by Zhou and Bhatt [16], and the method has proven to be very efficient for both first- and second-order phase transitions. It is also very useful in the study of systems with rough landscapes (such as the spin-glass problem) [12], because the algorithm has the property of maintaining a flat histogram in the random walk space. Applications of this method include simulations of fluids [17] (continuum systems), protein folding [18], polymer films [19], polymer collapse [20,21], binary Lennard-Jones glass [22], liquid crystals [23], random spin systems [24,25], atomic clusters [26], optimization problems [27], combinatorial number theory [28], Blume-Capel model [29], and three-dimensional (3D) Potts model [30,31]. This method has been improved by using the N-fold way [32] and multibondic sampling [33], and it also has been generalized to perform quantum Monte Carlo simulations [34,35] and sampling along the reaction coordinates for a molecular system [36]. A rigorous derivation for off-lattice implementation of this algorithm was given in Ref. [37]. Further generalizations and studies of this sampling technique have also been carried out by several authors [15,38–43].

To overcome the barriers in both energy and order-parameter spaces, we must perform a two-dimensional (2D) random walk as it was done in the spin-glass problem [12]. We restrict $J_3/J=2$ in this paper (the qualitative nature of the phase diagram is unchanged for a wide range of ratios [9]); therefore the Hamiltonian in Eq. (1) can be rewritten as a sum of two parts,

$$H = -JE' - HM',$$

$$E' = \sum_{\langle ij \rangle} S_i S_j + 2 \sum_{\langle ijk \rangle} S_i S_j S_k,$$

$$M' = \sum_i S_i, \tag{2}$$

where E' is proportional to the energy due to the two- and three-body interactions, and M' is the microscopic magnetization of the system. We perform a 2D random walk in (E',M') space to estimate the density of states $g(E',M')$, which is defined as the number of spin configurations for any given E' and M'.

At the beginning of the simulation, the density of states is unknown, so we simply set $g(E',M')=1$ for all possible (E',M'). Then we begin a random walk in (E',M') space by choosing a site randomly and flipping its spin with a probability proportional to the inverse of the momentary density of states. If we denote in general terms $A'(E',M')$ and $A''(E'',M'')$ as the points before and after a spin is flipped, respectively, the transition probability from A' to A'' is

$$p(A' \to A'') = \min\left[\frac{g(A')}{g(A'')}, 1\right]. \tag{3}$$

If the point $A''(E'',M'')$ is accepted we multiply the existing density of states by a modification factor $f>1$, that is, $g(E'',M'') \to f \times g(E'',M'')$, and we update the histogram H_v of visited states, that is $H_v(E'',M'') \to H_v(E'',M'')+1$. If $A''(E'',M'')$ is not accepted, we update $g(E',M') \to f \times g(E',M')$ and $H_v(E',M') \to H_v(E',M')+1$.

We continue performing the random walk until the histogram is flat in (E',M') space. If we keep the random walk after that, the estimated density of states simply fluctuates around the true value for that system. The modification factor f introduces a systematic error for the estimated density of states $\ln[g(E',M')]$, with a magnitude that is proportional to $\ln(f)$. To reduce this source of error, we systematically reduce the modification factor to a finer one using a function like $f_{i+1}=f_i^{1/n}$ $(n>1)$. After the histogram is flat, we reset the histogram [that is, $H_v(E',M')=0$ for all (E',M')], and begin the next level random walk with the new factor f_{i+1}. We end the random walk when the modification factor is smaller than a predefined value [such as $f_{\text{final}}=\exp(10^{-8}) \simeq 1.000\,000\,01$ used here]. To speed up the convergence of the density of states to the true value, the initial modification factor was as large as $f=f_0=e \simeq 2.718\,28\cdots$, and $n=4$ in our simulations. We perform the random walk on all possible (E',M') space with a single computer processor. It takes from about a few minutes to 10 days on a 1.3 GHz Itanium2 processor to obtain $g(E',M')$ for the lattices with linear sizes $L=6$ to $L=42$ used here. Multiple independent random walks were performed for each lattice size in order to estimate the statistical error in the density of states and the thermodynamic quantities obtained from them. We performed nine independent random walks for each of the larger lattice sizes ($L=30$ to $L=42$). Because these are two-dimensional random walks the memory used by the program is quite large (up to 3.5 GB for $L=42$).

The number of total entries for the 2D density of states $g(E',M')$ for the current model is as large as 3.9×10^6 for $L=42$ and all simulations are performed with a single random walk over all possible (E',M') space. In contrast, the number of entries for the 1D density of states $g(E)$ is only about 6.6×10^4 for the $L=256$ Ising model [11].

We should point out that it is impossible to obtain a perfectly flat histogram, but a histogram may be considered flat if $H_v(E',M')$ for all possible (E',M') is not less than $x\%$ of the average histogram, where $x\%$ is chosen according to the size and complexity of the system and the desired accuracy of the density of states. However, in this work we use a less stringent criterion: the histogram is considered flat when the number of entries larger than or equal to 2000 remains unchanged for $L^2 \times 10^6$ spin-flip trials.

III. PHASE DIAGRAM AND ORDER PARAMETERS

With an accurate density of states $g(E',M')$ obtained at the end of the random walk, we can calculate thermodynamic quantities at any temperature T and external magnetic field H for the system with a Hamiltonian given by Eq. (1).

The spontaneous magnetization per lattice site, shown in Fig. 1(a) as a function of T and H, can be computed from the density of states $g(E',M')$ using

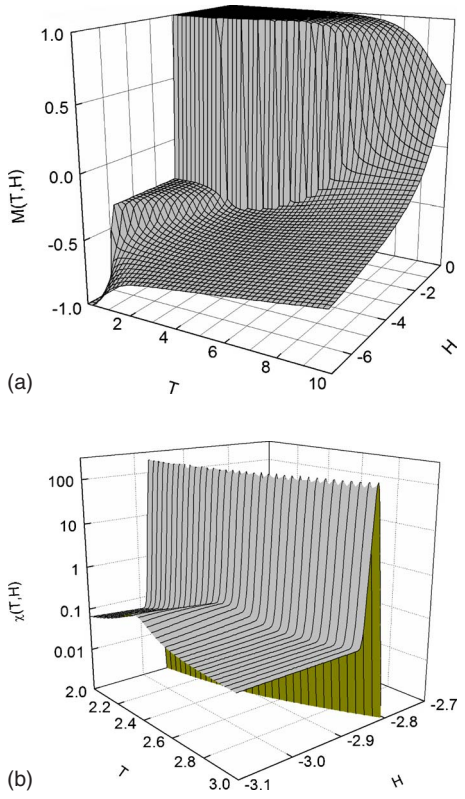

FIG. 1. (Color online) (a) Magnetization per site $M(T,H)$ and (b) susceptibility $\chi(T,H)$ calculated from the density of states $g(E',M')$ for $L=30$. Note that (b) is shown with a finer T and H scale than (a).

$$M(T,H) = \langle M \rangle = \frac{\sum_{E',M'} M' g(E',M') e^{-(-JE'-HM')/k_B T}}{N \sum_{E',M'} g(E',M') e^{-(-JE'-HM')/k_B T}}, \quad (4)$$

where we assume $J=1>0$ (ferromagnetic coupling), $N=L^2$ is number of lattice sites, and T is in unit of $1/k_B$ (k_B is the Boltzmann constant).

The susceptibility $\chi(T,H)$ also can be calculated from the density of states by

$$\chi(T,H) = dM/dH = N(\langle M^2 \rangle - \langle M \rangle^2)/k_B T. \quad (5)$$

The resulting $\chi(T,H)$ is shown in Fig. 1(b).

Our simulational data for magnetization and susceptibility show that the phase diagram has three distinct phases, each of which can be characterized by the values of the magnetization at $T=0$. The phases are phase A$(+++)$ with $M(0,H)=1$ (all spins are up), phase B$(---)$ with $M(0,H)=-1$ (all spins are down), and a ferrimagnetic phase C$(--+)$ with $M(0,H)=-1/3$ (the spins on two sublattices are down, the spins on the other sublattice are up). The phase boundaries can be determined, for example, by the locations of the maximum of the susceptibility.

Though the spontaneous magnetization is a good parameter to characterize the three phases, $M(T,H)$ is not the order parameter for the phase transitions because it does not vanish in any phase. For the transition between phase A and C as well as the transition between phase B and C, we define order parameters that are similar to those used for the $Q=3$ Potts model [44], because the degeneracy of the ground state in C phase is 3. For the Ising model discussed in this paper, we define two components (P_1,P_2) and vector order-parameter P from the magnetizations per site M_1, M_2, and M_3 of the three sublattices

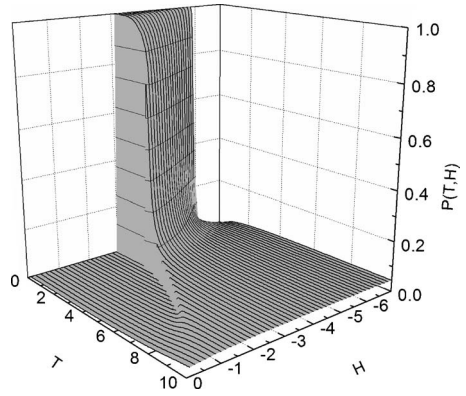

FIG. 2. Magnitude of the order-parameter $P(T,H)$ calculated from the density of states $g(E',M')$ for $L=30$.

$$P_1 = \frac{1}{2}\left(M_1 - \frac{M_2+M_3}{2}\right),$$

$$P_2 = \frac{\sqrt{3}}{4}(M_2 - M_3),$$

$$P = \sqrt{P_1^2 + P_2^2}. \quad (6)$$

$P_1(T,H)$, $P_2(T,H)$, and $P(T,H)$ approach zero in phases A$(+++)$ and B$(---)$, and finite values in phase C$(--+)$.

To calculate thermodynamic quantities $P(T,H)$, we must accumulate microscopic $P(E',M')$ during the random walk in the (E',M') space. If $P(E',M')$ is the microscopic average value during the random walk at (E',M'), the thermodynamic quantity $P(T,H)$ can be calculated as

$$P(T,H) = \frac{\sum_{E',M'} P(E',M') g(E',M') e^{-(-JE'-HM')/k_B T}}{\sum_{E',M'} g(E',M') e^{-(-JE'-HM')/k_B T}}. \quad (7)$$

A plot of $P(T,H)$ for $L=30$ is shown in Fig. 2, where the first- and second-order phase boundaries can be seen clearly. Figure 3(a) shows the phase diagram in the T and H plane extrapolated for $L=\infty$. The phase transition lines are determined by the locations where the susceptibility $\chi_p(T,H)$, defined as

$$\chi_p(T,H) = N(\langle P^2 \rangle - \langle P \rangle^2)/k_B T, \quad (8)$$

has its maximum value for a given fixed T and L. The finite lattice "phase transition lines" are then extrapolated to $L=\infty$ using finite-size scaling. Alternatively, the phase diagram can be obtained by the maximum of other thermodynamic

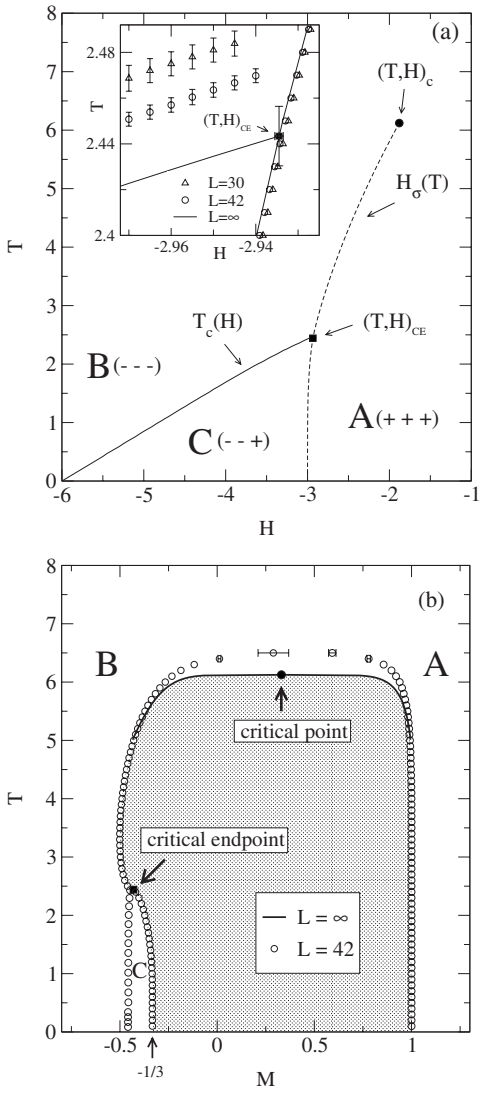

FIG. 3. (a) Phase diagram in the (T,H) plane extrapolated to $L=\infty$. The solid line is a critical line and the dashed line is a first-order phase transition line. The inset shows the region near the critical endpoint and includes data for $L=30$ (triangles) and $L=42$ (circles) to illustrate the finite-size effects (both phase transition lines extrapolated to $L=\infty$ are shown as solid lines in the inset). (b) Phase diagram in the (T,M) plane, showing data for $L=42$ and extrapolation to $L=\infty$. The shaded area is a region of phase coexistence.

quantities that show singularities along the phase boundaries, such as the specific heat, susceptibilities dM/dH, dP_1/dH, dP_2/dH, etc.

Our data for magnetization in Fig. 1(a) and susceptibility in Fig. 1(b), indicate that the transitions between phases A and B as well as between A and C are of first order [dashed line in Fig. 3(a)]. In contrast, the phase transition between B and C is of second order [solid line in Fig. 3(a)]. The critical endpoint, $(T,H)_{\mathrm{CE}}$, is defined at the point where the second-order critical line $T_c(H)$ meets, and is truncated by the first-order transition line $H_\sigma(T)$ beyond which the system transforms into a noncritical phase A (also called a spectator phase [1]). [The notation $H_\sigma(T)$ for the first-order transition line is more convenient than $T_\sigma(H)$, because we take temperature derivatives of this line in the analyses below.] At the end of $H_\sigma(T)$ is a critical point $(T,H)_c$. The solid circle in Fig. 3(a) is the location of $(T,H)_c$ for $L=\infty$. For a finite lattice the location of the peak in $\chi_p(T,H)$ extends well beyond the infinite lattice critical point; however, beyond T_c the peak does not diverge as $L\to\infty$.

Our extrapolated simulational results $H_c(T=0)=-6$ and $H_\sigma(T=0)=-3$ are consistent with the exact solutions at zero temperature and earlier simulational data [9]. We determine the critical line $T_c(H)$ separating phase B and C with great accuracy, except when this line reaches the CE. It is very difficult to determine $T_c(H)$ near the CE, because the peak in $\chi_p(T,H)$ corresponding to this phase transition merges with, and cannot be easily distinguished from, a larger peak due to the strong first-order transition. This is especially problematic for small lattices, but the larger L considered here were also affected somewhat. Nevertheless, $T_c(H)$ is a smooth line and we extend it from lower values of H to where it meets the first-order transition line. In the inset of Fig. 3(a) we see that for $L=42$ the critical line $T_c(H)$ must be extended from $H\approx-2.94$ to where it meets $H_\sigma(T)$. We then take this meeting point as an estimate of the critical endpoint for the finite lattice L. The phase diagram in the thermodynamic limit [solid lines in the inset of Fig. 3(a)] is obtained by extrapolating the phase transition lines for $L=30,33,36,42$ to $L=\infty$. The critical endpoint for $L=\infty$ is estimated as $(T,H)_{CE}=(2.443\pm0.010,-2.934\pm0.010)$.

Figure 3(b) is a plot of the phase diagram in the (T,M) plane, showing the critical magnetization per site along the critical line $T_c(H)$ and the peak locations of the magnetization distribution for the first-order line $H_\sigma(T)$. The shaded area corresponds to the coexistence between phases A and B for $T>T_{\mathrm{CE}}$ and between phases A and C for $T<T_{\mathrm{CE}}$. The open symbols correspond to $L=42$ and the solid line is an extrapolation to $L=\infty$ as described below. Here we have shown the $L=42$ phase diagram for T extending beyond the $L=\infty$ critical point $(T,H)_c$ to illustrate the finite size effects.

Although the main focus of this work is to study the critical endpoint, for completeness, we also performed a field mixing analysis [45,46] of the model to precisely determine the critical point at the end of the spectator phase boundary $H_\sigma(T)$. This analysis is performed with the mixed fields τ and h that are linear combinations of T and H, given by $\tau=T-T_c+s(H-H_c)$ and $h=H-H_c+r(T-T_c)$, and the corresponding conjugate scaling operators. Our estimate of the 2D Ising-type critical point is $(T,H)_c=(6.125\pm0.003, -1.879\pm0.002)$. The field mixing analysis also allows us to estimate the $L=\infty$ values of the magnetization at $(T,H)_c$ $(M_c=0.33\pm0.01)$ and near it [shown, respectively, as the solid circle and the solid line in Fig. 3(b)].

With the density of states $g(E',M')$ obtained at the end of the random walk, we can calculate thermodynamic quantities at any T and H without multiple simulations. Therefore, the phase boundaries can be determined continuously in the parameter space and with high accuracy. The flat histogram in the (E',M') space helps our simulations overcome the barriers in both energy and magnetization spaces. Because of

these barriers, it is very difficult to apply conventional Monte Carlo algorithms to this problem [5]. Though the multicanonical method [6] could overcome such barriers, we still would need to perform multiple simulations for different T and H (and use them with histogram reweighting [7]) in order to compute the curvature of the phase boundary accurately. Moreover, before a multicanonical simulation could be performed, an estimate of the density of states itself would be needed; this is a difficult task because of the free energy barriers for this problem.

IV. SINGULARITY AT THE CRITICAL ENDPOINT

The spectator phase boundary $H_\sigma(T)$ is obtained by the peak position of $\chi_p(T,H)$ for a given T. In order to obtain a smooth $H_\sigma(T)$ curve, we compute $\chi_p(T,H)$ in a very fine grid in the (T,H) plane (we used $dT=0.01$ and $dH=0.0001$). We then perform a least squares fitting around the peak in $\chi_p(T,H)$ for fixed T to determine the value of H (not necessarily one of the values in the H grid) for which $\chi_p(T,H)$ has a maximum. With an accurate estimate of the phase boundaries, we can calculate the curvatures of the spectator phase boundary $H_\sigma(T)$. In Fig. 4(a), the curvatures $d^2H_\sigma(T)/dT^2$ of the spectator phase boundary show a very clear singularity at the CE.

According to a general finite-size scaling argument [1,8], this curvature should diverge at the CE with a specific heatlike form

$$\left.\frac{d^2H_\sigma(T,L)}{dT^2}\right|_{\mathrm{CE}} = a_1 L^{\alpha/\nu} + a_2, \tag{9}$$

where α and ν are critical exponents defined on the critical line $T_c(H)$ and a_2 is a background. For the model we discuss in this paper, the critical exponents along $T_c(H)$ are in the same universality class as the 2D $Q=3$ Potts model because the two models have the same symmetry. Therefore, the predicted scaling exponent [see Eq. (9)] is $\alpha/\nu=2/5$, where we have used the conjectured values $\alpha=1/3$ and $\nu=5/6$ for the 2D $Q=3$ Potts model [47].

Figure 4(b) shows a log-log plot of the maximum of d^2H_σ/dT^2, denoted as $f(L)$, as a function of the linear lattice size L. The scaling relation is obtained by a linear fitting of the data for $L=18$ to 42 to Eq. (9), with a_1 and a_2 as fitting parameters and with the exponent fixed at $\alpha/\nu=2/5=0.4$. The fitted solid line shown in the inset of Fig. 4(b) has a slope of $a_1=0.106(8)$ and an intercept with the vertical axis $a_2=-0.11(3)$. The solid line in Fig. 4(b) shows the finite-size scaling relation of $f(L)$ using these fitted coefficients. Because we obtained quite a good fit to the scaling function $f(L)=a_1L^{0.4}+a_2$ [solid line in Fig. 4(b) and its inset] we can conclude that our data are in good agreement with the predicted scaling exponent [see Eq. (9)], but the background term is not negligible. Our data also indicate that there are small correction terms to the finite-size scaling; nevertheless, the resolution of our data and the lattice sizes used here are not adequate to estimate these correction terms. For a binary fluid mixture, Wilding [8] observed a clear divergence of the curvature of the spectator phase boundary; however the system sizes he used in his simulations were much too small to attempt a determination of the finite-size scaling exponent.

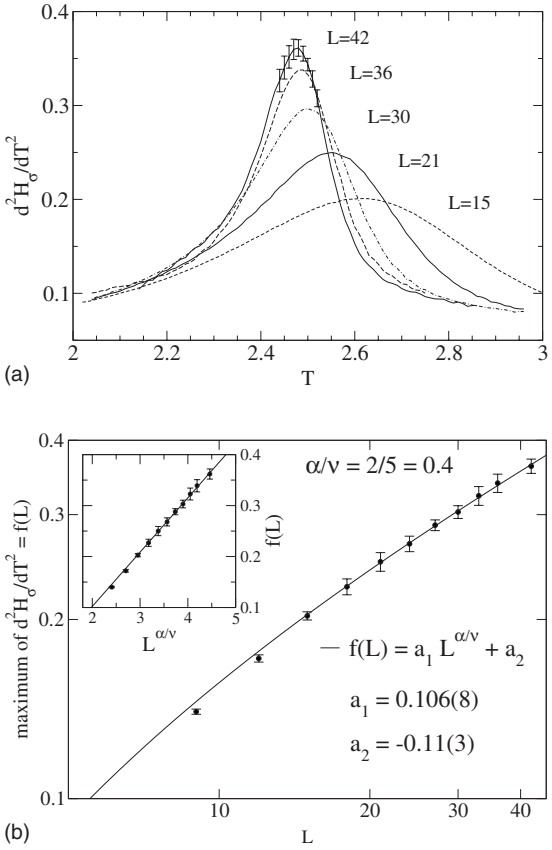

FIG. 4. (a) Singularity of the curvature d^2H_σ/dT^2 of the spectator phase boundary H_σ and (b) the finite-size scaling of the maximum of this curvature, which we denote $f(L)$. For clarity, in (a) we only show a few of the larger error bars for $L=42$. (Other error bars are smaller, particularly away from the peaks.) The inset of (b) shows a linear plot of $f(L)$ versus $L^{\alpha/\nu}=L^{0.4}$. The solid line in the inset is a linear fitting of the data.

The magnetization coexistence diameter M_d is defined as the average magnetization along the first-order transition line $H_\sigma(T)$. We obtain $M_d(T,H)$ using Eq. (4) where the parameters (T,H) are taken from the $H_\sigma(T)$ line. Using generalized scaling arguments, Wilding [8] predicted that the coexistence diameter derivative diverges as

$$\left.\frac{dM_d(T,H)}{dT}\right|_{\mathrm{CE}} = c_1 L^{\alpha/\nu} + c_2 L^{(1-\beta)/\nu}, \tag{10}$$

where α, β, and ν are critical exponents defined on the critical line $T_c(H)$. We observe a clear divergence of the derivative of the magnetization coexistence diameter [see Fig. 5(a)] near the critical endpoint. Figure 5(b) shows the scaling of the maximum of $-dM_d/dT$ with lattice size L. The solid line in Fig. 5(b) is a least squares fitting of the maximum of dM_d/dT using Eq. (10) with $L=15$ to 42 data. For the symmetric binary fluid studied by Wilding [8], the coefficient c_2 in Eq. (10) is predicted to vanish; therefore dM_d/dT should diverge with $L^{\alpha/\nu}$ at the CE. For the asymmetric model studied here, our data indicate that dM_d/dT at the CE does not

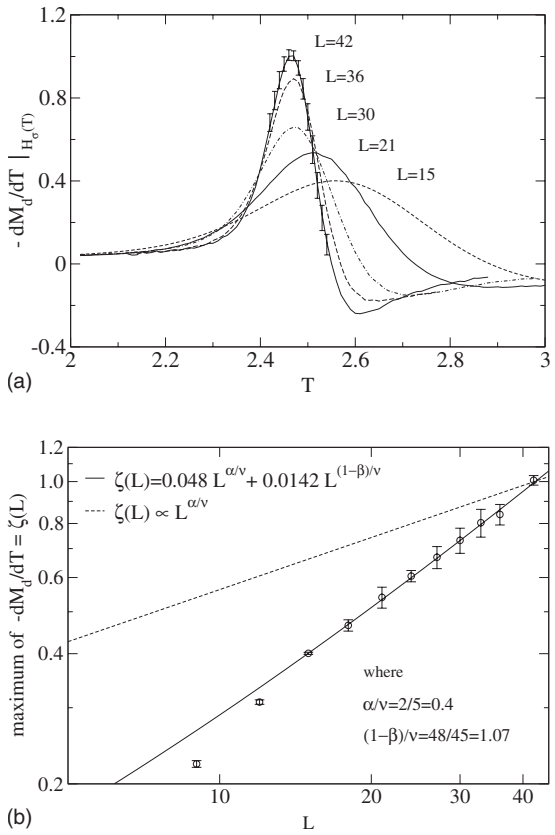

FIG. 5. (a) Singularity of the magnetization coexistence diameter $-dM_d/dT$ along H_σ and (b) the finite-size scaling of the maximum of this derivative. For clarity, in (a) we only show a few of the larger error bars for $L=42$. (Other error bars are smaller, particularly away from the peaks.)

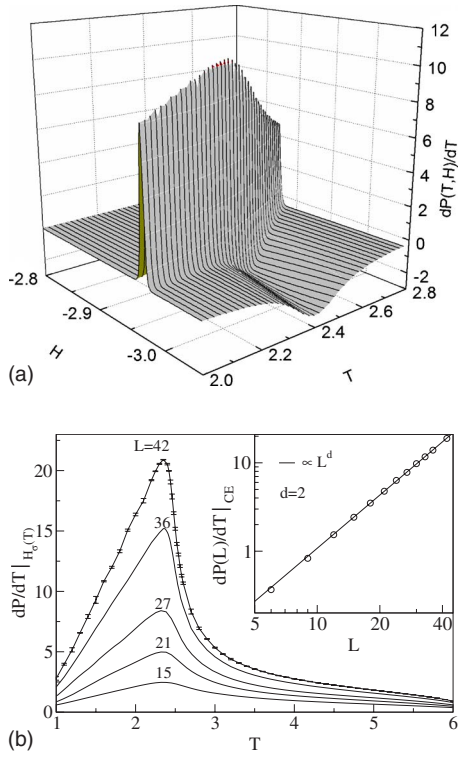

FIG. 6. (Color online) (a) 3D plot for the dP/dT calculated from the density of states for $L=30$. (b) Singularities of the dP/dT along the spectator phase boundary $H_\sigma(T)$, and finite-size behavior of dP/dT at the critical endpoint (inset). For clarity, in (b) we only show typical error bars for the larger lattice size. (Error bars for other L are smaller than the ones shown for $L=42$.) The error bars in the inset of (b) are not larger than the symbol sizes.

diverge with $L^{\alpha/\nu}$ [see the dashed line in Fig. 5(b)], whereas using both terms on the right-hand side of Eq. (10) yields a good fit to our data.

With the density of states $g(E',M')$, we can calculate dP/dT very easily at any temperature T and in any external field H. The resultant dP/dT, shown in Fig. 6(a), has a singularity at the CE. To show this singularity in detail, in Fig. 6(b) we only plot dP/dT along the spectator boundary for several L. The order-parameter jump dP/dT has a clear singularity at the CE. Both dP_1/dT and dP_2/dT also show a behavior similar to dP/dT.

Our data in the inset of Fig. 6(b) can be fitted well with

$$\left.\frac{dP(L)}{dT}\right|_{H_\sigma(T)} = cL^d, \tag{11}$$

where $d=2$ is the dimension of the lattice. This indicates that the finite-size dependence of $dP(L)/dT$ is dominated by the first-order nature of the $H_\sigma(T)$ transition line. The critical behavior between phases B and C is very difficult to study at the CE for finite-size systems because the first-order phase transitions are so strong. However, the singularities of dP/dT along the spectator phase boundary, and of $d^2H_\sigma(T)/dT^2$ and dM_d/dT are very clearly due to the critical transitions between the phases B and C.

V. SINGULARITY ALONG THE SPECTATOR PHASE BOUNDARY $H_\sigma(T)$

For the first-order phase transitions along $H_\sigma(T)$, finite-size analysis indicates that both at and away from the CE the maximum of thermodynamics quantities are proportional to L^d for finite-size systems (where d is the dimensionality of the lattice). In particular, the susceptibility $\chi=dM/dH$ and the specific heat C scale as

$$\chi(L)|_{H_\sigma(T)} \propto L^d,$$

$$C(L)|_{H_\sigma(T)} \propto L^d. \tag{12}$$

Figures 7(a) and 7(b) show the susceptibility and the specific heat, respectively, along $H_\sigma(T)$ for several lattice sizes. The insets in these figures confirm that the scaling relations in Eq. (12) are satisfied both at the CE and away from it (e.g., at $T=0.6T_{CE}$ and at $T=2T_{CE}$).

VI. SINGULARITY ALONG THE CRITICAL LINE $T_c(H)$

The critical line $T_c(H)$ for this asymmetric Ising model should be in the same universality class as the two-dimensional $Q=3$ Potts model, because the two models have the same symmetry. We recall that the conjectured values

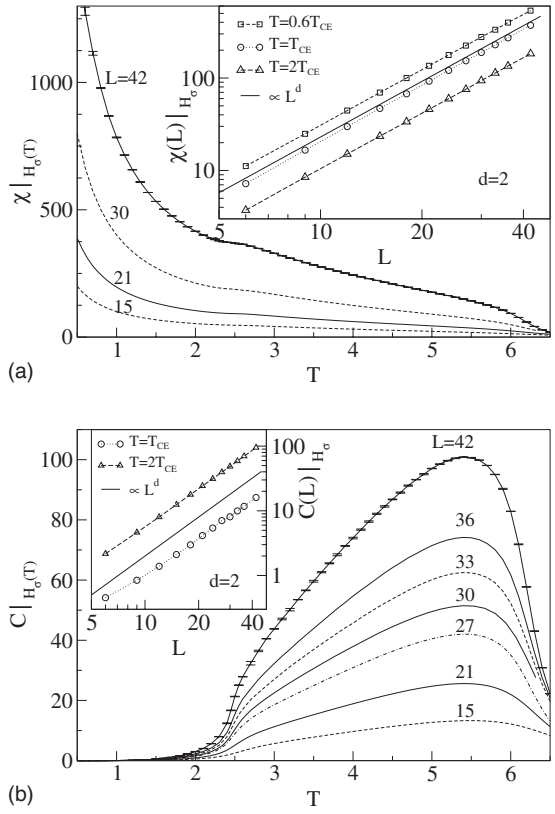

FIG. 7. Dependence of (a) the susceptibility $\chi=dM/dH$ and (b) the specific heat on T along the first-order phase transition line $H_\sigma(T)$ for several lattice sizes. The insets show the singularity in the respective thermodynamic quantities at $T=T_{\mathrm{CE}}$ and away from it along $H_\sigma(T)$. For clarity, we only show typical error bars for the larger lattice size. (Error bars for other L are smaller than the ones shown for $L=42$.) The error bars in the insets are not larger than the symbol sizes.

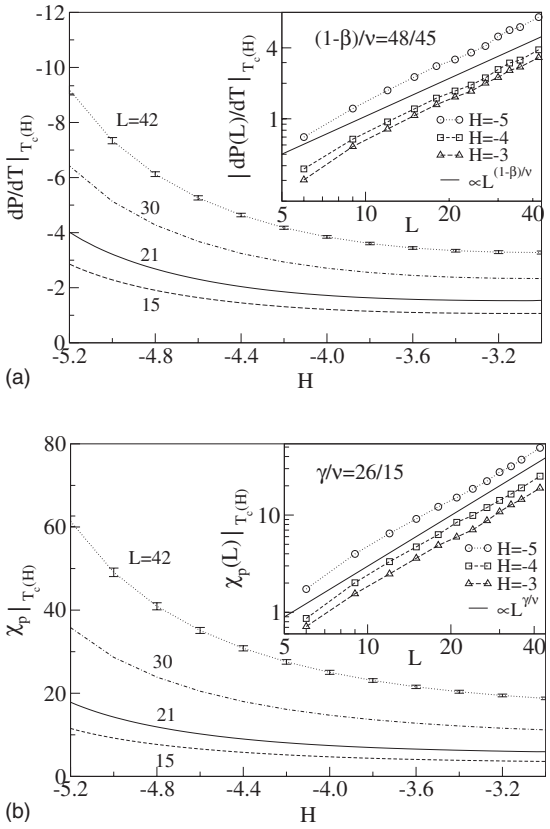

FIG. 8. Dependence of (a) dP/dT and (b) χ_p on H along the critical line $T_c(H)$ for several lattice sizes. The insets show the singularity in the respective thermodynamic quantities for three values of H along $T_c(H)$. For clarity, we only show typical error bars for the larger lattice size. (Error bars for other L are smaller than the ones shown for $L=42$.) The error bars in the insets are not larger than the symbol sizes.

[47] for the critical exponents of the latter model are $\alpha=1/3$, $\beta=1/9$, $\gamma=13/9$, and $\nu=5/6$. In order to verify that our data are consistent with these conjectured exponents, we study finite size scaling of derivatives of the order parameter along $T_c(H)$. Because the order-parameter P behaves as $P(T)\propto|[T-T_c(H)]/T_c(H)|^\beta$ near the critical line $T_c(H)$, the finite-size behavior of dP/dT at $T_c(H)$ is

$$\left.\frac{dP(L)}{dT}\right|_{T_c(H)} \propto L^{(1-\beta)/\nu}. \tag{13}$$

The finite-size scaling behavior of the susceptibility χ_p at the critical line is

$$\chi_p(L)|_{T_c(H)} \propto L^{\gamma/\nu}. \tag{14}$$

Figure 8(a) shows dP/dT along $T_c(H)$ for several lattice sizes. Characteristic error bars shown for the $L=42$ data are obtained from several independent runs. In the inset of Fig. 8(a), our simulational data for dP/dT versus L at three critical points in a wide region of external field ($H=-5$, -4, and -3) can be fitted well to the scaling form in Eq. (13) with $(1-\beta)/\nu=48/45\simeq 1.07$, where we used the conjectured critical exponents for the 2D $Q=3$ Potts model [47].

The susceptibility χ_p along $T_c(H)$ is shown in Fig. 8(b) for several values of L. The finite-size behavior of χ_p in the inset of Fig. 8(b) for different values of H scale well according to the relation given in Eq. (14), using the 2D $Q=3$ Potts critical exponents $\gamma/\nu=(13/9)/(5/6)\simeq 1.73$. The finite-size scaling shown in the insets of Figs. 8(a) and 8(b) confirms that the transition between phase C$(--+)$ and phase B$(---)$ is in the same universality class as the 2D $Q=3$ Potts model. Moreover, these results show that the critical exponents do not change when we approach the critical endpoint along the critical line $T_c(H)$.

VII. CONCLUSION

In summary, we use an efficient two-dimensional random walk algorithm, known as the Wang-Landau method, to estimate the density of states $g(E',M')$ of an asymmetric Ising model with two- and three-body interactions on a triangular lattice, in an external field. With an accurate estimate of $g(E',M')$ we were able to calculate thermodynamic quantities at any temperature T and in any external field H. We mapped out the phase diagram of this model and observe a clear divergence of the curvature of the spectator phase

boundary and of the magnetization coexistence diameter derivative at the critical endpoint. The exponents for both divergences agree well with the predicted values; however, the finite-size scaling for the divergence of the curvature of the spectator phase boundary includes a non-negligible background term. Our data suggest that there are small corrections to finite-size scaling and an accurate estimate of these terms requires using much larger system sizes. The nature of the behavior of the system near the critical endpoint was very well determined using finite-size scaling without having to determine the value of the critical endpoint to six significant digits.

Our finite-size analysis shows that the singularity for dP/dT at the critical endpoint is not different from the first-order phase transitions along the spectator phase boundary. We also provide numerical evidence that the critical exponents of the transition between phases B and C do not change when we approach the critical endpoint along the critical line. Thermodynamic quantities along the first-order line are shown to scale with lattice size as L^d both at and away from the critical endpoint.

ACKNOWLEDGMENTS

The authors thank K. Binder, C. K. Hu, H. Meyer, M. Müller, J. A. Plascak, J. S. Wang, and N. Wilding for helpful discussions and comments. Part of the simulations were performed on an Itanium cluster at SDSC and on an SGI Altix at the Research Computing Center at UGA. This work is supported in part by NSF Grant No. DMR-0341874.

[1] M. E. Fisher and P. J. Upton, Phys. Rev. Lett. **65**, 2402 (1990); **65**, 3405 (1990); M. E. Fisher, Physica A **172**, 77 (1991).
[2] T. A. L. Ziman, D. J. Amit, G. Grinstein, and C. Jayaprakash, Phys. Rev. B **25**, 319 (1982).
[3] See, for example, J. S. Rowlinson and B. Widom, *Molecular Theory of Capillarity* (Clarendon, Oxford, 1982); B. Widom, J. Phys. Chem. **77**, 2196 (1973), and references therein.
[4] M. E. Fisher and M. C. Barbosa, Phys. Rev. B **43**, 11177 (1991); M. C. Barbosa and M. E. Fisher, *ibid.* **43**, 10635 (1991); M. C. Barbosa, *ibid.* **45**, 5199 (1992).
[5] D. P. Landau and K. Binder, *A Guide to Monte Carlo Methods in Statistical Physics*, 2nd ed. (Cambridge University Press, Cambridge, 2005).
[6] B. A. Berg and T. Neuhaus, Phys. Rev. Lett. **68**, 9 (1992).
[7] A. M. Ferrenberg and R. H. Swendsen, Phys. Rev. Lett. **61**, 2635 (1988); **63**, 1195 (1989).
[8] N. B. Wilding, Phys. Rev. Lett. **78**, 1488 (1997); Phys. Rev. E **55**, 6624 (1997).
[9] K. K. Chin and D. P. Landau, Phys. Rev. B **36**, 275 (1987).
[10] S.-H. Tsai, F. Wang, and D. P. Landau, Braz. J. Phys. **36**, 635 (2006).
[11] F. Wang and D. P. Landau, Phys. Rev. Lett. **86**, 2050 (2001).
[12] F. Wang and D. P. Landau, Phys. Rev. E **64**, 056101 (2001).
[13] D. P. Landau and F. Wang, Comput. Phys. Commun. **147**, 674 (2002).
[14] D. P. Landau, S.-H. Tsai, and M. Exler, Am. J. Phys. **72**, 1294 (2004).
[15] B. J. Schulz, K. Binder, M. Müller, and D. P. Landau, Phys. Rev. E **67**, 067102 (2003).
[16] C. Zhou and R. N. Bhatt, Phys. Rev. E **72**, 025701(R) (2005).
[17] Q. Yan, R. Faller, and J. J. de Pablo, J. Chem. Phys. **116**, 8745 (2002); T. S. Jain and J. J. de Pablo, *ibid.* **118**, 4226 (2003).
[18] N. Rathore and J. J. de Pablo, J. Chem. Phys. **116**, 7225 (2002); N. Rathore, T. A. Knotts, and J. J. de Pablo, *ibid.* **118**, 4285 (2003).
[19] T. S. Jain and J. J. de Pablo, J. Chem. Phys. **116**, 7238 (2002).
[20] F. Rampf, K. Binder, and W. Paul, J. Polym. Sci., Part B: Polym. Phys. **44**, 2542 (2006).
[21] D. F. Parsons and D. R. M. Williams, Phys. Rev. E **74**, 041804 (2006); J. Chem. Phys. **124**, 221103 (2006).
[22] R. Faller and J. J. de Pablo, J. Chem. Phys. **119**, 4405 (2003).
[23] E. B. Kim, R. Faller, Q. Yan, N. L. Abbott, and J. J. de Pablo, J. Chem. Phys. **117**, 7781 (2002).
[24] Y. Okabe, Y. Tomita, and C. Yamaguchi, Comput. Phys. Commun. **146**, 63 (2002).
[25] Y. Wu and J. Machta, Phys. Rev. B **74**, 064418 (2006).
[26] F. Calvo and P. Parneix, J. Chem. Phys. **119**, 256 (2003).
[27] M. A. de Menezes and A. R. Lima, Physica A **323**, 428 (2003).
[28] V. Mustonen and R. Rajesh, J. Phys. A **36**, 6651 (2003).
[29] C. J. Silva, A. A. Caparica, and J. A. Plascak, Phys. Rev. E **73**, 036702 (2006).
[30] C. Yamaguchi and Y. Okabe, J. Phys. A **34**, 8781 (2001).
[31] Y. Okabe and H. Otsuka, J. Phys. A **39**, 9093 (2006).
[32] B. J. Schulz, K. Binder, and M. Müller, Int. J. Mod. Phys. C **13**, 477 (2002).
[33] C. Yamaguchi and N. Kawashima, Phys. Rev. E **65**, 056710 (2002).
[34] M. Troyer, S. Wessel, and F. Alet, Phys. Rev. Lett. **90**, 120201 (2003).
[35] P. N. Vorontsov-Velyaminov and A. P. Lyubartsev, J. Phys. A **36**, 685 (2003).
[36] F. Calvo, Mol. Phys. **100**, 3421 (2002).
[37] M. S. Shell, P. G. Debenedetti, and A. Z. Panagiotopoulos, Phys. Rev. E **66**, 056703 (2002).
[38] Q. Yan and J. J. de Pablo, Phys. Rev. Lett. **90**, 035701 (2003).
[39] N. Rathore, Q. Yan, and J. J. de Pablo, J. Chem. Phys. **120**, 5781 (2004).
[40] E. A. Mastny and J. J. de Pablo, J. Chem. Phys. **122**, 124109 (2005).
[41] A. Malakis, A. Peratzakis, and N. G. Fytas, Phys. Rev. E **70**, 066128 (2004); A. Malakis, S. S. Martinos, I. A. Hadjiagapiou, N. G. Fytas, and P. Kalozoumis, *ibid.* **72**, 066120 (2005); A. Malakis and N. G. Fytas, *ibid.* **73**, 056114 (2006); **73**, 016109 (2006).
[42] C. Zhou, T. C. Schulthess, S. Torbrügge, and D. P. Landau, Phys. Rev. Lett. **96**, 120201 (2006).
[43] H. K. Lee, Y. Okabe, and D. P. Landau, Comput. Phys. Commun. **175**, 36 (2006).
[44] Y. Tomita and Y. Okabe, Phys. Rev. Lett. **86**, 572 (2001); K.

Binder, K. Vollmayr, H.-P. Deutsch, J. D. Reger, M. Scheucher, and D. P. Landau, Int. J. Mod. Phys. C **3**, 1025 (1992).

[45] See, for example, N. B. Wilding and A. D. Bruce, J. Phys.: Condens. Matter **4**, 3087 (1992); N. B. Wilding, Phys. Rev. E **52**, 602 (1995), and references therein.

[46] J. A. Plascak and D. P. Landau, Phys. Rev. E **67**, 015103(R) (2003).

[47] F. Y. Wu, Rev. Mod. Phys. **54**, 235 (1982).